Jet Substructure in Fireworks Emission from Nonuniform and Rotating Bose-Einstein Condensates

Han Fu,[1,2,*] Zhendong Zhang,[1,2,3] Kai-Xuan Yao,[1,2,3] Lei Feng,[1,2,3] Jooheon Yoo,[2] Logan W. Clark,[1,2,3] K. Levin,[1,2] and Cheng Chin[1,2,3]

[1]James Franck Institute, University of Chicago, Chicago, Illinois 60637, USA
[2]Department of Physics, University of Chicago, Chicago, Illinois 60637, USA
[3]Enrico Fermi Institute and Department of Physics, University of Chicago, Chicago, Illinois 60637, USA

(Received 10 February 2020; accepted 14 September 2020; published 30 October 2020)

We show that jet emission from a Bose condensate with periodically driven interactions, also known as "Bose fireworks", contains essential information on the condensate wave function, which is difficult to obtain using standard detection methods. We illustrate the underlying physics with two examples. When condensates acquire phase patterns from external potentials or from vortices, the jets display novel substructure, such as oscillations or spirals, in their correlations. Through a comparison of theory, numerical simulations, and experiments, we show how one can quantitatively extract the phase and the helicity of a condensate from the emission pattern. Our work, demonstrating the strong link between jet emission and the underlying quantum system, bears on the recent emphasis on jet substructure in particle physics.

DOI: 10.1103/PhysRevLett.125.183003

Cold atom systems are emerging as an important platform for quantum simulations in condensed matter [1] and in high energy physics [2]. In this context, the application of temporal periodic drive has led to novel phenomena [3,4], including topological phases [5,6] and dynamical gauge fields for simulation of high-energy physics models [7–9]. With driven Bose-Einstein condensates (BECs), a new regime of quantum scattering has appeared [10–12], where periodic variations of the atomic interactions excite pairs of atoms propagating in opposite directions. With sufficiently strong modulations, thin jets of atoms are expelled from the condensate in all directions. This Bose stimulation (Bose fireworks) reveals complex correlations [13–16] and allows simulation of Unruh radiation [17] and density wave formation [18,19].

In this Letter, we show how this jet emission pattern can enable extraction of the condensate wave function. Such studies of jet substructure are reminiscent of current scattering experiments in particle physics performed at both the Large Hadron [20] and the Relativistic Heavy Ion [21] Colliders. It should be pointed out, in this regard, that vorticity (a topic of interest here) is an active subfield in particle physics [22]. Quark-gluon plasmas exhibiting anomalously high vorticity have been reported based on the structure of the particle emission. To illustrate this capability with cold atoms, a set of emission patterns from numerical simulations are shown in Fig. 1, which exhibit distinct structures for condensates with different nonuniform phase configurations.

We present two cases of study, both experimentally and numerically. In the first, we consider condensates split into two halves with different phases. The relative phase emerges in the correlations of counterpropagating jets and can be understood based on the double-slit interference of matter waves. In the second case, we study condensates with vortices. Here the emission pattern exhibits a novel spiral substructure as seen in Fig. 1(b). We show that one can directly extract the phase winding number of the vortices from the spirals. Excellent agreement between experiments and simulations is obtained for both cases.

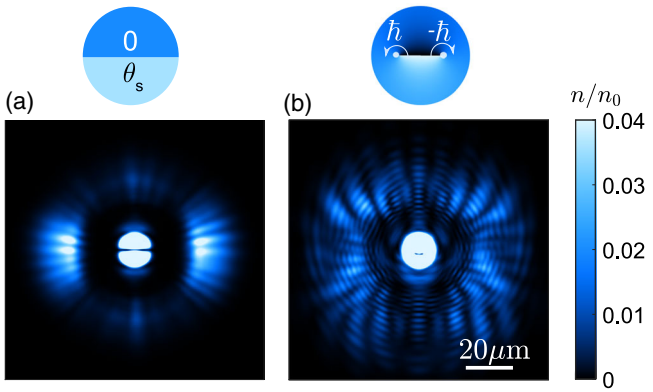

FIG. 1. Simulated emission patterns of BECs with interaction modulations. (a) Jet emission from condensates with a soliton. The lower half is phase shifted relative to the upper half by $\theta_s = \pi$. (b) Jet emission from condensates with a vortex-antivortex pair, where the reduced Planck constant $\hbar$ corresponds to the angular momentum of the vortex. The atomic density n is normalized to the initial density of the condensate n_0.

Our study shows jet emission as a new tool to probe the phase distribution of a condensate. We take vortex detection as an example. Time of flight [23] or *in situ* imaging [24] does not reveal the helicity (the phase winding) of the vortex, while the interference experiments do reveal the helicity but require preparation of two samples [25–27]. Our method uses only a single condensate (like Ref. [28]) to reveal the BEC phase distribution from the emitted atoms and can, in principle, be implemented with little disturbance of the condensate.

In our simulations, we describe the evolution of the condensates with the Gross-Pitaevskii (GP) equation, including terms that simulate quantum fluctuations [18]. For a uniform BEC, periodic modulation of the interaction strength with frequency ω leads to pair production of matter wave jets with random but opposite momenta $(\hbar\mathbf{k_f}, -\hbar\mathbf{k_f})$, where $k_f = \sqrt{m\omega/\hbar}$ and m is the atomic mass. For nonuniform condensates, jets form in pairs of modes, which are determined by the condensate wave function and driving frequency. When observed in the plane wave basis, the jets can show intricate correlations. The goal of this Letter is to demonstrate that much can be learned about the condensate from the strength and correlations of the emitted jets.

Microscopically, the system under the periodic drive is excited from an initial state ψ_0 to $\psi(t) \equiv \psi_0 + \delta\psi$, where the wave function increment $\delta\psi$ can be seeded by quantum fluctuations and amplified by the drive. With short interaction times as in our experiment, the deviation can be treated perturbatively, and the evolution of the system is governed by the Hamiltonian

$$H \approx \sum_i E_i a_i^\dagger a_i + \frac{U(t)}{2}\sum_{i,i'}[F(i,i')a_i^\dagger a_{i'}^\dagger + \text{H.c.}], \quad (1)$$

where $U(t) = U_0 + U_1 \sin\omega t$ is the oscillating interaction strength, $\sum_i$ sums over the single particle modes φ_i that are initially unoccupied, the pair function $F(i,i')$ is described below, E_i is the kinetic energy of the ith mode, and a_i and $a_i^\dagger$ are the annihilation and creation operators of the mode. Here we work in the regime where the modulation amplitude is much larger than the offset, and the driving energy is much greater than the energy of the initial state, i.e., $U_0 n_0 \ll U_1 n_0 \ll \hbar\omega$, where n_0 is the average density of the condensate [29].

The pair function $F(i,i')$ in Eq. (1) determines the strength as well as the correlations of the two modes i and i' in the emission. It is given by the overlap of the condensate wave function ψ_0 and the wave functions of the modes φ_i and $\varphi_{i'}$, namely,

$$F(i,i') = \int d\mathbf{r}\varphi_i^*(\mathbf{r})\varphi_{i'}^*(\mathbf{r})\psi_0^2(\mathbf{r}). \quad (2)$$

This equation shows that, in principle, we can determine the square of the condensate wave function directly from the pair function F. As an example, if we choose a plane wave basis, $F(\mathbf{k},\mathbf{k}')$ is the $\mathbf{k}+\mathbf{k}'$ Fourier component of ψ_0^2. When the condensate contains multiple excitations, those with larger amplitudes of $F(\mathbf{k},\mathbf{k}')$ will lead to stronger emission of the matter wave jets with momenta $\mathbf{k}$ and $\mathbf{k}'$, providing they satisfy momentum conservation conditions. The detailed mathematics needed to extract the pair function F and the experimental approach to implement the program is provided in the Supplemental Material [30]. To validate these ideas and offer a physical picture, we study two examples of nonuniform BECs experimentally and theoretically. These cases involve BECs with two different phases and with vortices, both of which illustrate the links between the jet substructure and condensate wave functions through the comparisons between experiments and simulations.

A split BEC with two phases is our first, pedagogical example. A solitonlike structure arises where the phase jump occurs and the condensate density is suppressed at the boundary. The advantage of considering a split BEC is that we are able to disentangle density and phase information, which are strongly intertwined in the soliton case. We assume that at time $t = 0$ the phase of the lower half is θ_s and that of the upper half is zero, and the phase slip boundary is along the horizontal direction.

To experimentally prepare this condensate with two phases, we start with a BEC of 4×10^4 cesium atoms in a circular box trap with diameter 18 μm [10]. The sample is tightly confined in the vertical direction with $1/e^2$ radius 0.8 μm. We then slowly raise a 6-μm wide potential barrier with a barrier height of $h \times 52$ Hz, thus maintaining phase coherence while substantially separating the BEC into two halves. A phase difference between the two halves is introduced by applying a short light pulse of duration $\tau = 0.4$ ms on one of them. The imprinted phase of $\theta_s = -V_s\tau/\hbar$, where V_s is the light shift, is controlled by the intensity of the light pulse. We calibrate the imprinted phase by interfering the two halves of the BEC after free expansion [30]. In the experiment, the potential barrier and the relative phase are controlled independently.

After phase imprinting, we apply an oscillating magnetic field in the vicinity of a Feshbach resonance to initiate the jet emission [10]. The magnetic field modulates the atomic s-wave scattering length as $a(t) = a_{\text{dc}} + a_{\text{ac}} \sin\omega t$ at frequency $\omega = 2\pi \times 2.1$ kHz with a small offset $a_{\text{dc}} = 9\, a_0$ and a large amplitude $a_{\text{ac}} = 47\, a_0$, where a_0 is the Bohr radius. The resulting chemical potential is around $h \times 89$ Hz. After the modulation, we perform imaging to record the jets. Emission patterns from experiments and from simulations based on identical parameters show good agreement, see Fig. 2(a). This figure illustrates the fact that the anisotropy in the emission pattern is caused by the density depletion. To see the relative phase, one needs to address the correlations.

We show below how this phase information can be quantitatively extracted. The phase difference between the

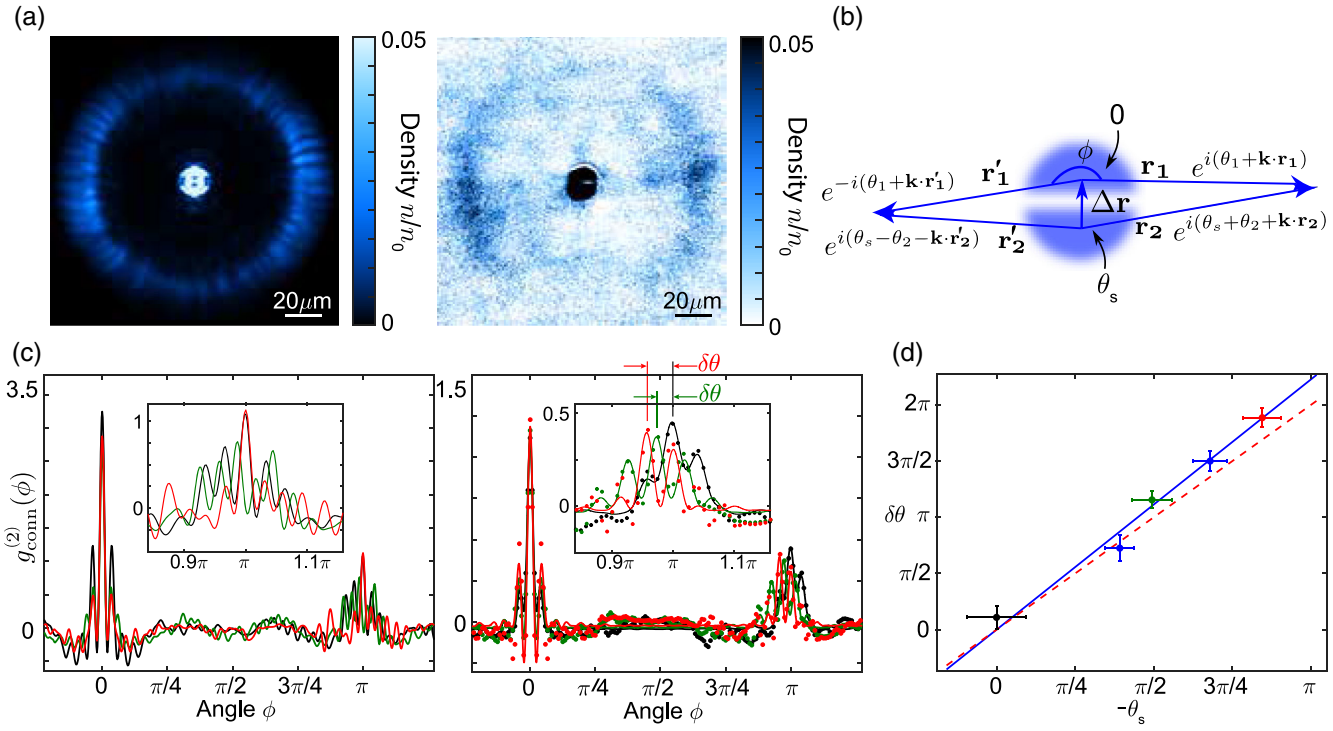

FIG. 2. Emissions from Bose condensates split into two halves with and without a relative phase θ_s. (a) Emission pattern for $\theta_s = 0$ from simulations (left) and experiments (right). The density is normalized by the initial average density n_0. (b) Physical picture for the jet emission from two halves of the condensate. (c) Connected correlations $g^{(2)}_{\rm conn}(\phi)$ for different relative angle ϕ (left: simulation; right: experiment) for $\theta_s = 0$ (black), $-\pi/2$ (green), and $-\pi$ (red). Solid lines are fits using the product of a sinc envelope and a sinusoidal function, borrowed from the double-slit interference model (see Supplemental Material, Sec. 2 [30]). The insets show the jet substructure of the π peaks. The phase shift $\delta\theta$ of the oscillations are indicated by the arrows. (d) Phase associated with π-peak shift $\delta\theta$ as a function of imprinted phase θ_s (plotted against $-\theta_s$). Dots with error bars are experimental data. The blue solid line is a linear fit without intercept and the red dashed line is the theory expectation $\delta\theta = -2\theta_s$, which is identical to the simulation results. Here, the data used in (c) are marked out with the same corresponding colors. Error bars represent 1-σ standard deviation.

two halves θ_s is revealed in the correlation between counterpropagating jets. We first calculate the connected correlation function $g^{(2)}_{\rm conn}$, defined as

$$g^{(2)}_{\rm conn}(\phi) = \frac{\langle \int_0^\pi d\phi_1 \Delta n_{\phi_1} \Delta n_{\phi_1+\phi} \rangle}{\pi \bar{n}^2}, \tag{3}$$

where $\Delta x = x - \langle x \rangle$ represents the fluctuation around the mean value, n_ϕ is the density of the emitted atoms at angle ϕ, $\langle\cdot\rangle$ denotes the average over all images, and $\bar{n}$ is the average density over all directions and images. The correlation function displays a strong peak at $\phi \approx \pi$, called the π peak, which indicates that jets form in pairs in opposite propagating directions.

Close examination shows that the π peak contains fine oscillations (jet substructure) that depend on the condensate phase, see Fig. 2(c). The phase of the oscillations is found to be proportional to the relative phase between the two halves θ_s. Comparing the phase $\delta\theta$ of the fine oscillations to the phase difference θ_s, we find a linear dependence with a slope $-2.2(2)$, see Fig. 2(d). Although there is an uncertainty in the experiments that reflects calibration errors in the imprinted phase, these measurements are consistent with the theoretical prediction

$$\delta\theta = -2\theta_s. \tag{4}$$

We provide an intuitive picture to understand this phase relation. In the far field, emission from the upper BEC with probability amplitude $e^{i(\theta_1+\mathbf{k}\cdot\mathbf{r_1})}$ propagating to the right overlaps with the emission from the lower half with amplitude $e^{i(\theta_s+\theta_2+\mathbf{k}\cdot\mathbf{r_2})}$, where θ_1 and θ_2 are random phases determined by quantum fluctuations, $\mathbf{k}$ is the jet wave vector, and $\mathbf{r_1}$ ($\mathbf{r_2}$) is the displacement vector toward the measurement point, see Fig. 2(b). The two matter waves interfere and produce a density wave of $\cos(\Delta\theta - \theta_s + \mathbf{k}\cdot\Delta\mathbf{r})$, where $\Delta\theta = \theta_1 - \theta_2$ and $\Delta\mathbf{r} = \mathbf{r_1} - \mathbf{r_2}$. Similarly, the left-propagating emissions of amplitudes $e^{i(-\theta_1-\mathbf{k}\cdot\mathbf{r_1'})}$ and $e^{i(\theta_s-\theta_2-\mathbf{k}\cdot\mathbf{r_2'})}$ overlap and result in a density wave $\cos(\Delta\theta + \theta_s + \mathbf{k}\cdot\Delta\mathbf{r})$ [32]. Comparing the two density waves, we see that the counterpropagating emissions are correlated with a relative phase shift of $\delta\theta = -2\theta_s$.

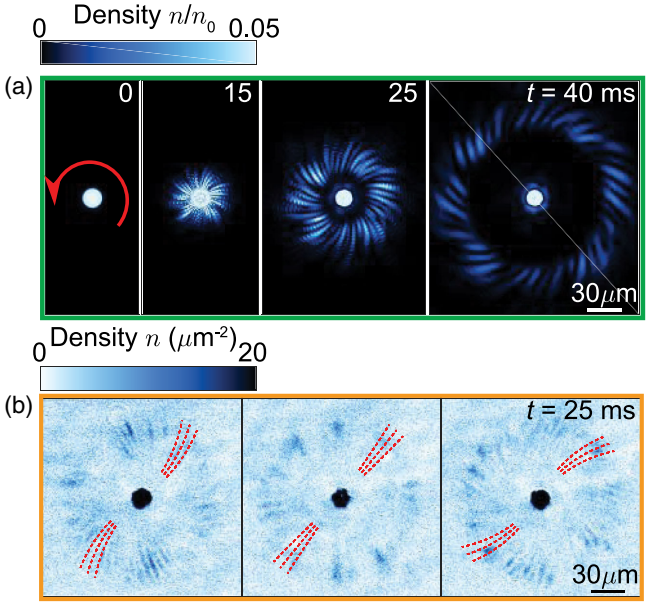

FIG. 3. Spiral emissions from vortex-embedded BECs. (a) Evolution of the fireworks emission for $\omega/2\pi = 2$ kHz and $l_0 = 1$ from GP simulation. The red arrow indicates the direction of the phase winding with $l_0 = 1$. (b) Experimental images for $\omega/2\pi = 3$ kHz at $t = 25$ ms from BECs with different vortex winding numbers $l_0 = -1, 0, 1$ from left to right. The red dashed lines are guides to the eye, the curvature of which is calculated from the correlation function [30].

The second case study involves vortex-embedded BECs, where the resulting emission patterns display exotic spirals. In our system, the initial condensate wave function is characterized by an integer winding number $l_0 = \pm 1, \pm 2, \ldots$ as

$$\psi_0(r, \phi) = \sqrt{n_0(r)} e^{i l_0 \phi} \tag{5}$$

in polar coordinates (r, ϕ). Since the healing length ξ (set by the chemical potential μ as $\hbar^2/2m\xi^2 = \mu$) is much smaller than the trap radius R, the condensate wave function is uniform outside the vortex core. Jet emission dynamics from a driven BEC with a vortex is simulated in Fig. 3(a).

In our experiment, about 5% of condensates form with a vortex, arising from the finite cooling time in transition to condensation [33–35]. When the system reaches equilibrium, the vortex is expected to settle at the trap center. BECs with and without a vortex can be distinguished using the emission pattern; see Fig. 3(b) for emission from BECs with different vorticity [30].

Our simulations and experiments show a consistent picture that the jet emission displays a spiral pattern in the presence of vorticity in the BEC. When the winding number is positive, the spirals are clockwise. The spiral emission pattern is the key observable that determines the winding number of the condensate.

This spiral pattern can be understood based on a semiclassical picture. Considering atoms inside the rotating condensate as independent emitters, an atom has a unique momentum $\mathbf{k}$ of magnitude l_0/r along the transverse direction. When two such atoms collide inelastically, they are excited to new momenta $\mathbf{k} \pm \mathbf{k_f}$, where $|\mathbf{k_f}| = k_f$. For an observation point outside the sample, jets emitted from different parts ("sources") of the condensate overlap and interfere, and the observed spirals are the resulting interference fringes.

To see the connection between the direction of the spiral and the angular momentum, we note that, when the observer moves away from the condensate, the phase of the matter wave with relatively large momentum accumulates faster. Thus, the interference fringes curves toward the jet with the higher momentum, namely, $\mathbf{k} + \mathbf{k_f}$, to maintain the same interference condition, see Fig. 4(a). Theoretical analysis suggests $d\phi/dr = -\eta l_0/(k_f R^2)$ [30], with η being a dimensionless constant. This equation describes the observed spirals.

To test these predictions, we evaluate the correlation function between two points with radial distance r and angular distance ϕ, namely,

$$g_t^{(2)} = \frac{\int d\phi' dr' \langle n(r', \phi') n(r' + r, \phi' + \phi) \rangle}{2\pi L_0 \tilde{n}^2}, \tag{6}$$

where the integration of r' covers the interval L_0 that jets manifest [36], and $\tilde{n}$ is the mean density in the interval.

The spiral pattern associated with the jet substructure can be understood as representing a linear relation between the radial and angular distances in the emission; see Fig. 4(b), where the red dashed lines show linear fits to the correlations involving r and ϕ. This linear dependence suggests that the emission emerges with an effective angular velocity $\omega_e = -(\hbar k_f/m) d\phi/dr$, which can be compared with the winding number of the condensate according to

$$\omega_e = \eta \frac{l_0 \hbar}{m R^2}, \tag{7}$$

see Fig. 4(c). From simulations, we determine $\eta = 2.90$ for $l_0 = \pm 1$ and $\eta = 2.19$ for $l_0 = \pm 2$. We speculate that the decrease of η for larger $|l_0|$ is a result of the instability of a vortex-containing BEC with $l_0 = \pm 2$. A vortex with $l_0 = 2$ will quickly decay into two vortices with $l_0 = 1$, and the finite spatial separation between them reduces the effective angular velocity. For a classical, rigid uniform disk with the same radius R, we expect that the angular velocity is $\omega_e = \eta_{\rm cl} l_0 \hbar/(mR^2)$ with $\eta_{\rm cl} = 2$.

The same analysis on the experimental data also yields a linear relationship between r and ϕ in the correlation function. Based on multiple repeated experiments, we find that ηl_0 takes on quantized values of $\eta l_0 = -3.07(3)$, $-0.10(6)$, and $3.0(1)$, which are in very good agreement

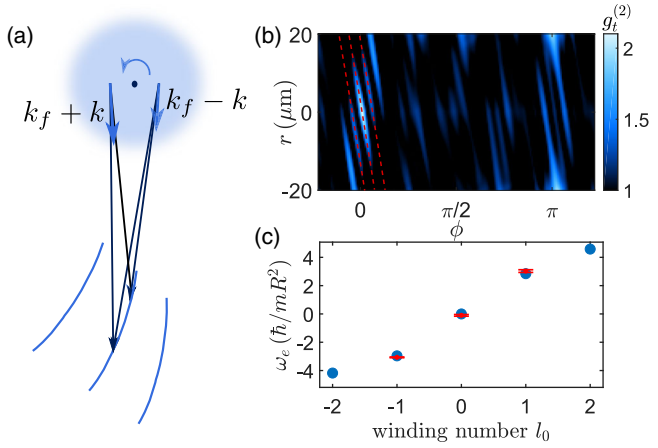

FIG. 4. Correlation analysis of spiral emission patterns. (a) A physical picture to explain the origin of the spiral patterns from a rotating BEC as interference fringes from matter wave emitters with different momenta, see text. (b) Correlation functions $g_t^{(2)}$ in polar coordinates (r, ϕ) for $t = 40$ ms image in Fig. 3(a). Red dashed lines show linear fits to the correlations between r and ϕ. (c) Effective angular velocity ω_e, expressed in units of $\hbar/mR^2$, for condensates with different winding number l_0. Blue circles are from simulations and red circles are from experiments. Error bars represent 1-σ standard deviation.

with the simulation results for $l_0 = -1$, 0, and 1, see Fig. 4(c). The agreement between experiments and simulations confirms our scheme to reveal the helicity of a BEC directly from the jet emission pattern.

In conclusion, we present a methodology for extracting the phase distribution of a BEC based on jet emission. From the jet substructure of a driven BEC, one can determine the density and phase correlations and, in principle, reconstruct the pair function F of the condensate. The two illustrative examples discussed here show how one can recover the wave function phase information from the far field (split BECs) or near field (vortex-imbedded BECs) emission. In the far field, density-density correlators of jets can be directly obtained. In the near field, interference between adjacent jets reveals the relative phases of the jets [30]. Our experiments show excellent agreement with the theory and simulations. Remarkably, the jet substructure is an important observable in particle physics [20,21] to understand the dense systems formed in high-energy scattering experiments. Our analysis may offer a convenient test bed to determine the properties of a many-body sample with its attendant jet emission pattern.

We acknowledge Miguel Arratia, S. Fnu, and X. Wang for helpful discussions, and I. Aronson and A. Glatz for the numerical code. We acknowledge support by the U.S. Department of Energy, Office of Basic Energy Sciences, under Award No. DE-SC0019216, the Army Research Office under Grant No. W911NF-15-1-0113, and the University of Chicago Materials Research Science and Engineering Center, funded by the National Science Foundation under Grant No. DMR-1420709. L. F. acknowledges support from the University of Chicago Materials Research Science and Engineering Center Graduate Research Fellowship.

*vickeyrobert@uchicago.edu

[1] Q. Chen, J. Stajic, S. Tan, and K. Levin, Phys. Rep. **412**, 1 (2005).
[2] M. Arratia, J. Phys. B **52**, 055301 (2019).
[3] A. Eckardt, Rev. Mod. Phys. **89**, 011004 (2017).
[4] N. R. Cooper, J. Dalibard, and I. B. Spielman, Rev. Mod. Phys. **91**, 015005 (2019).
[5] N. Goldman, J. C. Budich, and P. Zoller, Nat. Phys. **12**, 639 (2016).
[6] G. Jotzu, M. Messer, R. Desbuquois, M. Lebrat, T. Uehlinger, D. Greif, and T. Esslinger, Nature (London) **515**, 237 (2014).
[7] L. W. Clark, B. M. Anderson, L. Feng, A. Gaj, K. Levin, and C. Chin, Phys. Rev. Lett. **121**, 030402 (2018).
[8] C. Schweizer, F. Grusdt, M. Berngruber, L. Barbiero, E. Demler, N. Goldman, I. Bloch, and M. Aidelsburger, Nat. Phys. **15**, 1168 (2019).
[9] F. Görg, K. Sandholzer, J. Minguzzi, R. Desbuquois, M. Messer, and T. Esslinger, Nat. Phys. **15**, 1161 (2019).
[10] L. W. Clark, A. Gaj, L. Feng, and C. Chin, Nature (London) **551**, 356 (2017).
[11] L. Clark, Quantum many-body dynamics with driven Bose condensates: Kibble-Zurek mechanism and Bose fireworks, Ph.D. thesis, University of Chicago, 2017.
[12] T. Mežnaršič, R. Žitko, T. Arh, K. Gosar, E. Zupanič, and P. Jeglič, Phys. Rev. A **101**, 031601 (2020).
[13] L. Feng, J. Hu, L. W. Clark, and C. Chin, Science **363**, 521 (2019).
[14] Z. Wu and H. Zhai, Phys. Rev. A **99**, 063624 (2019).
[15] T. Chen and B. Yan, Phys. Rev. A **98**, 063615 (2018).
[16] L.-Y. Chih and M. Holland, New J. Phys. **22**, 033010 (2020).
[17] J. Hu, L. Feng, Z. Zhang, and C. Chin, Nat. Phys. **15**, 785 (2019).
[18] H. Fu, L. Feng, B. M. Anderson, L. W. Clark, J. Hu, J. W. Andrade, C. Chin, and K. Levin, Phys. Rev. Lett. **121**, 243001 (2018).
[19] Z. Zhang, K.-X. Yao, L. Feng, J. Hu, and C. Chin, Nat. Phys. **16**, 652 (2020).
[20] R. Kogler *et al.*, Rev. Mod. Phys. **91**, 045003 (2019).
[21] M. Connors, C. Nattrass, R. Reed, and S. Salur, Rev. Mod. Phys. **90**, 025005 (2018).
[22] L. Adamczyk *et al.*, Nature (London) **548**, 62 (2017).
[23] J. R. Abo-Shaeer, C. Raman, J. M. Vogels, and W. Ketterle, Science **292**, 476 (2001).
[24] K. E. Wilson, Z. L. Newman, J. D. Lowney, and B. P. Anderson, Phys. Rev. A **91**, 023621 (2015).
[25] M. R. Matthews, B. P. Anderson, P. C. Haljan, D. S. Hall, C. E. Wieman, and E. A. Cornell, Phys. Rev. Lett. **83**, 2498 (1999).
[26] S. Inouye, S. Gupta, T. Rosenband, A. P. Chikkatur, A. Görlitz, T. L. Gustavson, A. E. Leanhardt, D. E. Pritchard, and W. Ketterle, Phys. Rev. Lett. **87**, 080402 (2001).

[27] L. Corman, L. Chomaz, T. Bienaimé, R. Desbuquois, C. Weitenberg, S. Nascimbène, J. Dalibard, and J. Beugnon, Phys. Rev. Lett. **113**, 135302 (2014).

[28] S. W. Seo, B. Ko, J. H. Kim, and Y. Shin, Sci. Rep. **7**, 4587 (2017).

[29] In the high-frequency limit, additional terms like $U(t)\int dxdy|\psi_0(x,y)|^2\varphi_i^*(x,y)\varphi_{i'}(x,y)$ are negligible, see Ref. [11].

[30] See Supplemental Material at http://link.aps.org/supplemental/10.1103/PhysRevLett.125.183003 for the mathematics needed to extract the pair function together with the experimental proposal. More details and analysis on the simulations and experimental procedures are also provided, which includes Ref. [31].

[31] M. Abramowitz and I. Stegun, *Handbook of Mathematical Functions* (Dover, New York, 1964).

[32] From Eq. (2) the phases of the jets emitted from the same half of the BEC sum to twice the phase of the BEC.

[33] L. Chomaz, L. Corman, T. Bienaimé, R. Desbuquois, C. Weitenberg, S. Nascimbène, J. Beugnon, and J. Dalibard, Nat. Commun. **6**, 6162 (2015).

[34] N. Navon, A. L. Gaunt, R. P. Smith, and Z. Hadzibabic, Science **347**, 167 (2015).

[35] J. Beugnon and N. Navon, J. Phys. B **50**, 022002 (2017).

[36] Assuming jets appear within $r_{\min} < r < r_{\max}$, we integrate r' in the range such that both measurement points at r' and $r' + r$ are within this ring area.